



Growth patterns for shape-shifting elastic bilayers

Wim M. van Rees^{a,1}, Etienne Vouga^b, and L. Mahadevan^{a,c,d,e,f,2}

^aJohn A. Paulson School of Engineering and Applied Sciences, Harvard University, Cambridge, MA 02138; ^bInstitute for Computational Engineering and Sciences, University of Texas at Austin, Austin, TX 78712; ^cWyss Institute for Biologically Inspired Engineering, Harvard University, Cambridge, MA 02138; ^dDepartment of Physics, Harvard University, Cambridge, MA 02138; ^eDepartment of Organismic and Evolutionary Biology, Harvard University, Cambridge, MA 02138; and ^fKavli Institute for NanoBio Science and Technology, Harvard University, Cambridge, MA 02138

Edited by John A. Rogers, Northwestern University, Evanston, IL, and approved September 6, 2017 (received for review May 31, 2017)

Inspired by the differential-growth-driven morphogenesis of leaves, flowers, and other tissues, there is increasing interest in artificial analogs of these shape-shifting thin sheets made of active materials that respond to environmental stimuli such as heat, light, and humidity. But how can we determine the growth patterns to achieve a given shape from another shape? We solve this geometric inverse problem of determining the growth factors and directions (the metric tensors) for a given isotropic elastic bilayer to grow into a target shape by posing and solving an elastic energy minimization problem. A mathematical equivalence between bilayers and curved monolayers simplifies the inverse problem considerably by providing algebraic expressions for the growth metric tensors in terms of those of the final shape. This approach also allows us to prove that we can grow any target surface from any reference surface using orthotropically growing bilayers. We demonstrate this by numerically simulating the growth of a flat sheet into a face, a cylindrical sheet into a flower, and a flat sheet into a complex canyon-like structure.

inverse physical geometry | growth | form | morphogenesis | 4D printing

Nonuniform in-plane growth of thin sheets generically leads to metric frustration that is relieved by out-of-plane buckling. This mechanism lies at the heart of many morphogenetic processes in botany, such as the shaping of a leaf (1), the blooming of a flower (2), or the explosive dispersal of seeds from certain pods (3). From an engineering perspective, these examples raise the possibility of biomimetic design: programming shape (morphogramming) into matter that can be actuated with environmental signals such as light, temperature, or concentration.

The theory of non-Euclidean plates and shells that links the elastic response of materials into the correctly invariant framework provided by differential geometry (1, 4–8) is a natural starting place to analyze the growth and form of sheets and shells. Growing a thin structure by changing the in-plane intrinsic distances and angles between material elements makes its metric non-Euclidean; generically, this implies that the strain-free reference configuration may not be physically realizable in 3D space. Therefore, the system settles into a residually strained equilibrium configuration that is determined by a local minimum of the energetic cost of stretching and bending the sheet. Generally, this state might not be unique, and, typically, there will be a range of metastable configurations accessible to the system. This raises the natural question of the inverse problem: How should one program growth patterns into a sheet so that it morphs into a prescribed target shape? Recent attempts to solve this question have focused on theoretical designs of optimal growth patterns for the weakly nonlinear deformations of thin shape-shifting isotropic elastic sheets (9), axisymmetric growth patterns for morphable shells (10), design of director fields into deformable nematic elastic sheets (11), or a 4D phytomimetic printing approach based on a linearized elastic analysis to derive the print paths of an anisotropic bilayer made of a responsive ink (12). However, there is no general theoretical or computational framework to solve this inverse problem.

Here, we address this question in the context of a growing elastic bilayer, inspired by the growth and form of plant organs

such as leaves and flowers that are usually made of two cell layers that adhere to each other and can grow independently. This bilayer geometry may be naturally described in terms of an infinitesimally-thin “midsurface” and a “thickness” h that is amenable to a physical description as a thin elastic shell capable of in-plane growth. For very thin plates and shells, an asymptotically correct low-dimensional description of the solid can be used to justify the Kirchhoff–Love assumption, namely, that normals to the cross-section are inextensible and remain normal during deformations. Then, the shell volume is characterized at all times in terms of a solid that extrudes a short distance in the normal direction above and below the midsurface. We assume that growth (*i*) occurs only in the in-plane directions (tangent to the midsurface) and that (*ii*) the shell can be divided into several “layers,” with growth constant through the thickness direction for each layer. These assumptions allow us to represent growth within each layer as a tensor field specified at each point of the midsurface. “Isotropic growth” consists of an equal growth factor in all in-plane directions at every point, and is thus encoded by one independent degree of freedom (the isotropic scaling factor) per layer at each point on the midsurface. With “orthotropic growth,” the growth factor of the material at each point is a function of the in-plane direction, providing three degrees of freedom per layer for each location on the midsurface: the two growth factors in the orthogonal “principal growth directions” and the planar rotation angle of this axis. Given the ubiquity of the bilayer geometry in plant organs, and the ease of additive manufacturing techniques that allow us to approach this possibility, we will focus on this case from now on.

Such a bilayer where each of the two layers can experience independent orthotropic growth (Fig. 1, *Left*) has six degrees of

Significance

Many biological forms, such as leaves, flowers, and faces, are shaped by complex growth patterns. How can we prescribe the rules of growth on a simple surface so that it will morph into a flower or a face? Here, we solve this inverse problem of designing the growth patterns for an anisotropically growing elastic bilayer structure and prove that it can be used to achieve any target surface shape from any reference shape. We demonstrate the applicability of this result via the computational design of growth patterns for animal, vegetable, and mineral surfaces—a face, a flower, and a canyon. Our solution provides algorithms for engineering complex functional shapes in tissues, and actuation systems in soft robotics, and elsewhere.

Author contributions: L.M. conceived the study; W.M.v.R., E.V., and L.M. designed research; W.M.v.R. and E.V. performed research; W.M.v.R., E.V., and L.M. analyzed data; and W.M.v.R., E.V., and L.M. wrote the paper.

The authors declare no conflict of interest.

This article is a PNAS Direct Submission.

¹Present address: Department of Mechanical Engineering, Massachusetts Institute of Technology, Cambridge, MA 02139.

²To whom correspondence should be addressed. Email: lmahadev@g.harvard.edu.

This article contains supporting information online at www.pnas.org/lookup/suppl/doi:10.1073/pnas.1709025114/-DCSupplemental.

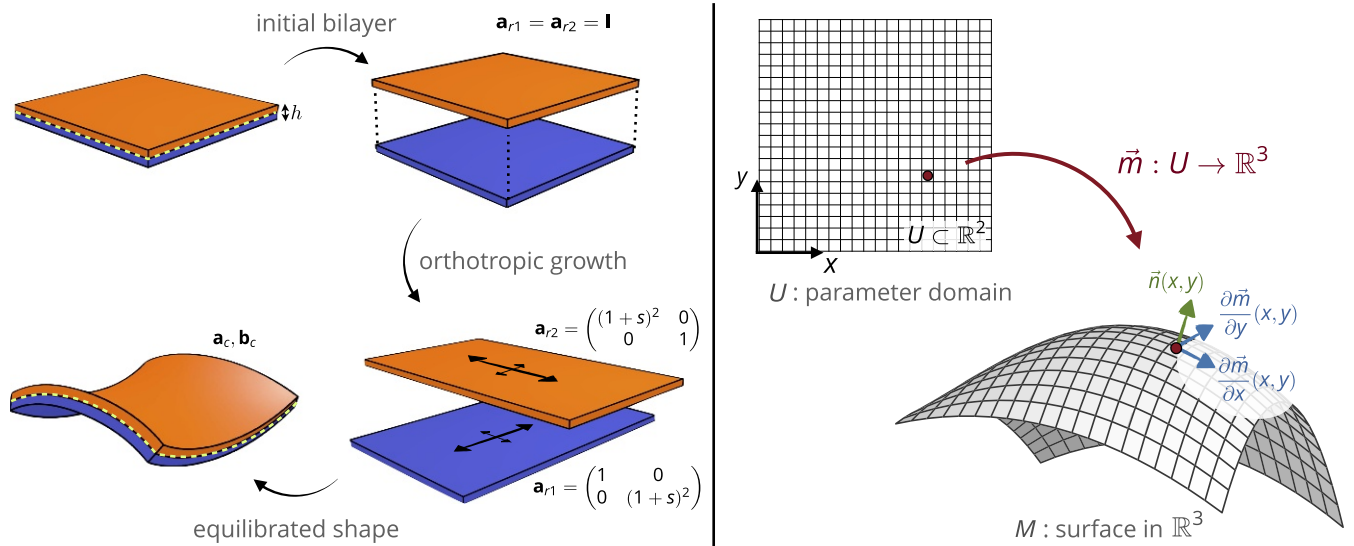


Fig. 1. (Left) A growing bilayer is considered as two independently, possibly inhomogeneously, growing layers, characterized by their own respective metrics \mathbf{a}_{r1} and \mathbf{a}_{r2} , that are glued together at a shared midsurface. In this example, each layer grows in only one direction, orthogonal to that of the other layer, with the linear growth factor $s > 0$. After each layer is grown, the bilayer embedding that minimizes the total elastic energy, characterized by first and second fundamental forms \mathbf{a}_c and \mathbf{b}_c , can be computed. (Right) The surface M is defined as an embedding $\vec{m} : U \rightarrow \mathbb{R}^3$ of an arbitrary region of the plane U into \mathbb{R}^3 . The embedding provides a normal field \vec{n} , as well as the first and second fundamental forms \mathbf{a}_c and \mathbf{b}_c , as described in the text.

freedom at every location along the common midsurface. Any choice of these degrees of freedom constitutes a growth field for the shell, giving rise to an equilibrium shape in \mathbb{R}^3 determined by minimizing the elastic energy of the composite. The design of the growth pattern to achieve a given target shape from an initial reference state leads to the formulation of the following inverse problem: Is it possible to find growth factors and directions for an orthotropically growing bilayer, so that its midsurface changes from a region of the plane or other simple shape initially, into some specified target surface after growth?

Classical differential geometry of 2D surfaces (13) tells us that a surface is uniquely defined by two symmetric quadratic forms (the first and second fundamental form), which consist of six quantities at every location along it. Naive counting of the degrees of freedom suggests that since we have three degrees of freedom associated with the in-plane growth of each of the layers in the composite bilayer, solutions to the inverse problem should be possible. In this work, we show that a solution does indeed always exist for the inverse problem when regularized as an elastic energy minimization problem. Furthermore, while this solution typically does not yield a resultant shape with zero residual strain (due to incompatibility when crossing from one layer to the other through the midsurface), we show that the residual strain is constant (i.e., independent of the realization of the bilayer). We provide a simple algebraic expression for the growth factors and angles that achieve this solution, allowing any bilayer to grow into any target shape.

Geometry and Elasticity

We parameterize the midsurface of a shell using curvilinear coordinates (x, y) in a domain U of the plane, and define its embedding in space by a map $\vec{m} : U \rightarrow \mathbb{R}^3$. Each point $\vec{m}(x, y)$ on the midsurface is characterized by its tangent vectors $\partial\vec{m}/\partial x$ and $\partial\vec{m}/\partial y$, and a normal unit vector $\vec{n} = (\partial\vec{m}/\partial x \times \partial\vec{m}/\partial y) / \|\partial\vec{m}/\partial x \times \partial\vec{m}/\partial y\|$, as shown in Fig. 1, Right. By using the Kirchhoff–Love assumption, any material point \vec{s} inside the volume of the shell can then be written in terms of a normal offset from the midsurface:

$$\vec{s}(x, y, z) = \vec{m}(x, y) + z\vec{n}(x, y),$$

where $z \in [-h/2, h/2]$, and h is the thickness of the shell. This map gives rise to a metric \mathbf{G} on the volume $U \times [-h/2, h/2]$

$$\mathbf{G}(x, y, z) = (d\vec{s})^T d\vec{s} = \begin{pmatrix} \mathbf{g}_c(x, y, z) & 0 \\ 0 & 1 \end{pmatrix},$$

with the 2×2 tensor \mathbf{g}_c defined as

$$\begin{aligned} \mathbf{g}_c(x, y, z) &\equiv (d\vec{m} + z d\vec{n})^T (d\vec{m} + z d\vec{n}) \\ &= \mathbf{a}_c(x, y) - 2z\mathbf{b}_c(x, y) + \mathcal{O}(z^2), \end{aligned}$$

where $\mathbf{a}_c = (d\vec{m})^T d\vec{m}$ and $\mathbf{b}_c = -(d\vec{m})^T d\vec{n} = -(d\vec{n})^T d\vec{m}$ are the first and second fundamental forms of the midsurface in the current configuration. The metric \mathbf{g}_c can be interpreted as measuring the lengths of tangent vectors on any offset surface normal to the midsurface, as well as the angles between them.

Similarly, we can describe the “growth” of U by prescribing a rest (unstrained) metric \mathbf{g}_r to each location in the shell. This rest metric can be written similarly:

$$\mathbf{g}_r(x, y, z) = \mathbf{a}_r(x, y) - 2z\mathbf{b}_r(x, y) + \mathcal{O}(z^2).$$

In general, the shell whose midsurface is described by this growth metric will not have a strain-free embedding in three dimensions, so that for any actual embedding, the shell will be subject to residual strain. To understand which embedding is then realized in physical space, we must therefore turn to a physical description of the shell as an elastic object.

Elastic Energy of a Curved Monolayer. Given the “rest quantities” U , \mathbf{a}_r and \mathbf{b}_r , we can compute for any map \vec{m} an elastic potential energy $E(\vec{m})$, so that \vec{m} is an equilibrium embedding of $(U, \mathbf{a}_r, \mathbf{b}_r)$ whenever $d_{\vec{m}}E = 0$ (i.e., whenever \vec{m} extremizes the elastic energy). Assuming a hyperelastic isotropic material constitutive model for the material of the shell (known as a St. Venant–Kirchhoff model), we can derive (see *SI Appendix* for details) the depth-integrated elastic energy as

$$\begin{aligned} E_{ML} = \frac{1}{2} \int_U &\left[\frac{h}{4} \|\mathbf{a}_r^{-1} \mathbf{a}_c - \mathbf{I}\|_e^2 \right. \\ &\left. + \frac{h^3}{12} \|\mathbf{a}_r^{-1} (\mathbf{b}_c - \mathbf{b}_r)\|_e^2 \right] \sqrt{\det \mathbf{a}_r} dx dy, \end{aligned} \quad [1]$$

where \mathbf{a}_e and \mathbf{b}_e are, respectively, the first and second fundamental form of the midsurface in its current realization (and so depend on \bar{m}). Here, the norm $\|\mathbf{A}\|_e^2 = \alpha \text{Tr}^2(\mathbf{A}) + 2\beta \text{Tr}(\mathbf{A}^2)$ defines the elastic constitutive law (14), with $\alpha = Y\nu/(1 - \nu^2)$ and $\beta = Y/(2 + 2\nu)$, where Y is the Young's modulus and ν the Poisson's ratio of the material. We note that this energy formulation contains the classical decomposition into a stretching energy term of $\mathcal{O}(h)$, penalizing the stretch and shear of the midsurface, and a bending energy term of $\mathcal{O}(h^3)$, measuring the resistance to curvature (15). Furthermore, for weakly nonlinear deformations this energy formulation is equivalent to the well-known Föppl–Von Karman formulation for thin elastic plates (see *SI Appendix* for details of this equivalence).

Elastic Energy of a Bilayer. A bilayer is made of two monolayers of thickness $h/2$ each, that have been ‘glued’ together at the shared midsurface. Each of the layers has its own independent first fundamental form given by \mathbf{a}_{r1} for the bottom and \mathbf{a}_{r2} for the top layer (Fig. 1, *Left*). Here, ‘bottom’ and ‘top’ are used with the convention of midsurface normal vectors pointing upward (i.e., into the layer whose metric is \mathbf{a}_{r2}).

The elastic energy of a bilayer made of two layers with metrics given by \mathbf{a}_{r1} and \mathbf{a}_{r2} , and a midsurface embedded in \mathbb{R}^3 with first and second fundamental forms \mathbf{a}_e and \mathbf{b}_e , can then be written as the sum of the energies of the individual layers. After integration over the depth of each layer, we obtain the energy as an integral over the common midsurface (*SI Appendix*)

$$E_{BL} = \frac{1}{2} \int_U \left[\frac{h}{8} \|\mathbf{a}_{r1}^{-1} \mathbf{a}_e - \mathbf{I}\|_e^2 + \frac{h^3}{24} \|\mathbf{a}_{r1}^{-1} \mathbf{b}_e\|_e^2 + \frac{h^2}{8} \langle (\mathbf{a}_{r1}^{-1} \mathbf{a}_e - \mathbf{I}), \mathbf{a}_{r1}^{-1} \mathbf{b}_e \rangle_e \right] \sqrt{\det \mathbf{a}_{r1}} dx dy + \frac{1}{2} \int_U \left[\frac{h}{8} \|\mathbf{a}_{r2}^{-1} \mathbf{a}_e - \mathbf{I}\|_e^2 + \frac{h^3}{24} \|\mathbf{a}_{r2}^{-1} \mathbf{b}_e\|_e^2 - \frac{h^2}{8} \langle (\mathbf{a}_{r2}^{-1} \mathbf{a}_e - \mathbf{I}), \mathbf{a}_{r2}^{-1} \mathbf{b}_e \rangle_e \right] \sqrt{\det \mathbf{a}_{r2}} dx dy, \quad [2]$$

where we have defined an elastic energy inner product $\langle \mathbf{A}, \mathbf{B} \rangle_e = \alpha \text{Tr}(\mathbf{A}) \text{Tr}(\mathbf{B}) + 2\beta \text{Tr}(\mathbf{AB})$. In the special case when the two monolayers grow exactly the same amount starting from a flat reference configuration, $\mathbf{a}_{r1} = \mathbf{a}_{r2} = \mathbf{a}_r$ so that this energy simplifies to the monolayer energy of Eq. 1.

Energy Equivalence Between Monolayers and Bilayers. A natural question that is raised by the geometric and mechanical description of the composite bilayer is whether we can relate it to an equivalent monolayer with appropriate first and second fundamental forms. In this work we show that, indeed, if \mathbf{a}_r and \mathbf{b}_r are appropriately expressed in terms of \mathbf{a}_{r1} and \mathbf{a}_{r2} , the energy of a monolayer can be related to the energy of a bilayer whenever they share the same realization of their midsurfaces.

To see this equivalence, consider the ansatz $\mathbf{a}_r = (\mathbf{a}_{r1} + \mathbf{a}_{r2})/2$ and $\mathbf{b}_r = \zeta(\mathbf{a}_{r1} - \mathbf{a}_{r2})/h$. The simple and natural choice $\zeta = 1/2$ has been proposed in ref. 3 and adopted in ref. 11; however, an analysis of the shell energetics suggests that this value is incorrect: Substituting the ansatz above into the expression for E_{BL} shows that the correct choice is actually $\zeta = 3/4$ as it yields the result (see *SI Appendix* for details)

$$E_{BL} = E_{ML} + \int_U \frac{h^3}{72} \|\mathbf{a}_{r1}^{-1} \mathbf{b}_r\|_e^2 \sqrt{\det \mathbf{a}_r} dx dy. \quad [3]$$

The last term on the right side corresponds to a strain that is independent of the embedding, since it does not depend on \mathbf{a}_e and \mathbf{b}_e . This result shows that the minimum-energy realization of a monolayer with reference quadratic forms

$$\mathbf{a}_r = \frac{1}{2}(\mathbf{a}_{r1} + \mathbf{a}_{r2}), \quad \mathbf{b}_r = \frac{3}{4h}(\mathbf{a}_{r1} - \mathbf{a}_{r2}), \quad [4]$$

is identical to that of a bilayer with \mathbf{a}_{r1} and \mathbf{a}_{r2} , allowing for a much simpler representation of the composite made of two elastic layers of the same thickness in terms of an energetically equivalent monolayer with curved reference configuration. The generalization to a bilayer with layers of unequal thicknesses and/or Young's moduli can be solved similarly, where Eqs. 3 and 4 become functions of h_1 , h_2 , Y_1 , and Y_2 , which define the thicknesses and Young's moduli of the bottom and top layer, respectively (see *SI Appendix* for details).

Forward Problem of Growth

The result of Eqs. 3 and 4 can be used to compute the quadratic forms \mathbf{a}_r and \mathbf{b}_r , defining the monolayer that is energetically equivalent to a bilayer with individual layer metrics \mathbf{a}_{r1} and \mathbf{a}_{r2} . However, for the corresponding midsurface to have a valid embedding in 3D space, we need to satisfy certain compatibility relations between the first and second fundamental forms. Those relations are given by three differential compatibility relations: the Gauss and Peterson–Mainardi–Codazzi equations (13). The six degrees of freedom of \mathbf{a}_r and \mathbf{b}_r , or equivalently \mathbf{a}_{r1} and \mathbf{a}_{r2} , together with these three differential relations, can be integrated to obtain the three components of \bar{m} at each location on the surface (up to rigid body motion), as specified by the Bonnet theorem (ref. 16, p. 236); see *SI Appendix* for the mathematical details of these constraints.

To give a sense of how this plays out practically, we consider two examples of the forward problem. First, consider the case of Fig. 1, *Left*, where we prescribed orthotropic growth to each of the layers, with the top layer growing in one principal direction and the bottom layer growing in the orthogonal direction. Both layers experience 1D expansion with the same, constant factor s , so that the affected metric entry for each of the layers gets scaled by $(1 + s)^2$. The quadratic forms of the energetically equivalent monolayer, \mathbf{a}_r and \mathbf{b}_r , are then given by Eq. 4. It is easy to see that these two forms, being spatially homogeneous, automatically satisfy both of the Peterson–Mainardi–Codazzi equations. Gauss' equation, however, cannot be satisfied: The Gauss curvature K of the suggested embedding is necessarily negative for any growth factor, whereas the derivatives of the metric \mathbf{a}_r are identically zero. This means that no surface with $\mathbf{a}_e = \mathbf{a}_r$ and $\mathbf{b}_e = \mathbf{b}_r$ can exist, as it would violate Gauss's Theorema Egregium (13). The equilibrium configuration in Fig. 1, *Lower Left* is therefore characterized by residual strain (see *SI Appendix* for details).

Second, consider a modification of the example of Fig. 1, where the two layers instead grow in the same direction, but with different growth factors s_1 and s_2 . For this case, the first and second fundamental forms \mathbf{a}_r and \mathbf{b}_r satisfy the compatibility relations identically, and correspond to a surface of zero Gauss curvature. Furthermore, if we assume small growth factors, we find that the nonzero principal curvature of the resulting surface is equal to $3/(2h)(s_1 - s_2)$. This result is identical to the classical analysis of Timoshenko (17) for the curvature of heated bimetallic strips, and the correspondence holds also for the case of unequal layer thicknesses and unequal layer Young's moduli (see *SI Appendix* for more details). Our solution, summarized in Eqs. 3 and 4, therefore not only generalizes Timoshenko's theory to nonlinear elasticity and arbitrary growth factors, but can also be seen as its extension that allows us to proceed from strips to surfaces.

Inverse Problem of Growth

As noted above, inhomogeneous orthotropic growth for each layer in the bilayer can be represented in terms of three degrees of freedom at every point—two growth factors corresponding to

the growth in orthogonal principal directions and one angle to define the axes. Together, these three values define the symmetric positive definite first fundamental form at a given location. For orthotropic growth of a bilayer, we therefore have independent control of the first fundamental forms for the bottom and top layer, which provides six degrees of freedom for each point on the surface. This leads to the following theorem:

Theorem 1. *Given any surface $M \subset \mathbb{R}^3$ and any shaped planar region $U \subset \mathbb{R}^2$ (topologically compatible with M) with embedding $\bar{m} : U \rightarrow \mathbb{R}^3$, so that the immersion of \bar{m} is equal to M , there exists a bilayer $(U, \mathbf{a}_{r1}, \mathbf{a}_{r2})$, with sufficiently small desired thickness h so that \bar{m} defines the energetically equilibrated configuration of the bilayer's midsurface. This bilayer is defined by*

$$\mathbf{a}_{r1} = \mathbf{a}_c + \frac{2h}{3}\mathbf{b}_c, \quad \mathbf{a}_{r2} = \mathbf{a}_c - \frac{2h}{3}\mathbf{b}_c, \quad [5]$$

where \mathbf{a}_c and \mathbf{b}_c are the first and second fundamental forms of M . Moreover, this embedding is free of residual strain, with the exception of a deformation-independent strain due to incompatibility of the bilayers at their common boundary. Finally, the metrics \mathbf{a}_{r1} and \mathbf{a}_{r2} as defined in Eq. 5 can be decomposed as orthotropic growth of a bilayer on U .

Proof. Eq. 3 states that the minimum energy embedding of a curved monolayer, with $\mathbf{a}_r = (\mathbf{a}_{r1} + \mathbf{a}_{r2})/2$ and $\mathbf{b}_r = 3(\mathbf{a}_{r1} - \mathbf{a}_{r2})/(4h)$, is identical to that of a bilayer with \mathbf{a}_{r1} and \mathbf{a}_{r2} . From Eq. 1 we can immediately see that the minimum energy configuration of a curved monolayer with embedding \bar{m} is achieved if $\mathbf{a}_r = \mathbf{a}_c$ and $\mathbf{b}_r = \mathbf{b}_c$. With \mathbf{a}_r and \mathbf{b}_r defined as such, we can solve for \mathbf{a}_{r1} and \mathbf{a}_{r2} of the bilayer using Eq. 4, resulting in Eq. 5. From Eq. 3, we can see that the resulting bilayer embedding is free of residual strain except for the already-mentioned deformation-independent term. Finally, by performing a spectral decomposition of the metric, we can write both \mathbf{a}_{r1} and \mathbf{a}_{r2} as orthotropic growth of a bilayer on U . \square

With this theorem, we have the capability to grow any initial bilayer structure into any target shape. However, we need to specify two practical considerations. First of all, the metrics \mathbf{a}_{r1} and \mathbf{a}_{r2} , defined by Eq. 5 have to be positive-definite to be admissible (13). We show in the *SI Appendix* that this results in the constraint

$$\max(|\kappa_1|, |\kappa_2|) < \frac{3}{2h},$$

where κ_1 and κ_2 are the principal curvatures of the target surface. In theory, this condition can always be met if the bilayer is thin enough, although in practice, manufacturing constraints on the thickness may limit the space of target shapes that can be grown.

Secondly, the trajectory of growth that is followed to transition from initial to final bilayer metrics might pose complications in practice. Although the embedding of the geometry that globally minimizes the energy given the final bilayer metrics is always unique and identical to the target configuration, some growth trajectories might result in a metastable shape different from the target shape. Since any metastable shape can always be “snapped” into the desired target shape, this issue is of secondary importance to our main contribution, yet provides some interesting questions. In particular, to guarantee that a growth process always results in the target shape, we anticipate two numerical and/or physical difficulties that could arise during interpolation of the metrics. First, it is important for the symmetric positive definite (SPD) matrices encoding the bilayer metrics to vary smoothly over time and remain SPD throughout the interpolation, and, moreover, for the eigenvectors and eigenvalues (encoding the anisotropy amount and direction) to vary as

smoothly as possible during interpolation. Second, interpolated bilayer metrics at intermediate growth stages should remain as compatible as possible; by this, we mean that the first and second fundamental form corresponding to the interpolated bilayer metrics should deviate as little as possible from satisfying the Gauss and Peterson–Mainardi–Codazzi compatibility relations. Otherwise, residual strain accumulates during the interpolation and could pose an energetic barrier between the final realized shape and the target solution. Again, the target solution would still be the global energetic minimum, but physically or numerically, we could find ourselves stuck at a local minimum. A particular numerical example of this is further detailed in the *SI Appendix*, for the case of the snapdragon flower growth case shown below.

A systematic approach to completely avoiding metastable states during the growth process is a very interesting direction for future work, and we can now pose the problem in a crisp way: Is it possible to interpolate two pairs of bilayer metrics, so that the equivalent minimum-energy midsurface fundamental forms are always compatible? Even more interesting is the prospect to harness incompatibility at intermediate growth stages to control the final grown shape, or exploit multiple solutions depending on the spatiotemporal distribution of growth, for instance, by snap-through (18).

Results

For parametrized surfaces, we can use Eq. 5 directly to solve the inverse problem algebraically. In simple situations associated with parametric surfaces that have explicit fundamental forms (e.g., a hemisphere, catenoid, and a saddle), we can carry out these computations analytically (*SI Appendix*). However, to truly demonstrate the usefulness of our approach, we need to show how to design growth patterns for complex shapes with multiple spatial scales. We do this by using numerical methods to minimize Eq. 2. For a given 3D target surface, we first triangulate it using a mesh that can capture the smallest length scale of interest, and then compute the current first and second fundamental forms \mathbf{a}_c and \mathbf{b}_c . We compute the first fundamental forms of the two layers that constitute the bilayer according to Eq. 5, and decompose each of them spectrally into local orthotropic growth rules for a given reference mesh and its corresponding bilayer metrics. We then interpolate the growth factors on each point in the initial mesh into a set of discrete values between those of the reference and target surfaces and solve a sequence of problems to determine the intermediate equilibrium configuration at each of the discrete growth steps. This provides a way to visualize the transition from initial to final configuration in a quasi-static manner, and further allows us to design arbitrary way-points between the initial and final state (*SI Appendix*).

Inspired by recent work on floral morphogenesis (19–21), we first show how we can grow a cylinder made of two thin sheets of the same uniform thickness into a snapdragon flower. In this case, we assume the initial cylinder, with \mathbf{a}^{CYL} and \mathbf{b}^{CYL} , is formed by a bilayer with growth factors $\mathbf{a}_{r1}^{\text{CYL}}$ and $\mathbf{a}_{r2}^{\text{CYL}}$, defined according to Eq. 5. The snapdragon flower, with \mathbf{a}^{SD} and \mathbf{b}^{SD} , is similarly represented by a bilayer with $\mathbf{a}_{r1}^{\text{SD}}$ and $\mathbf{a}_{r2}^{\text{SD}}$. To interpolate the reference first fundamental forms of the bilayer from $(\mathbf{a}_{r1}^{\text{CYL}}, \mathbf{a}_{r2}^{\text{CYL}})$ to $(\mathbf{a}_{r1}^{\text{SD}}, \mathbf{a}_{r2}^{\text{SD}})$, we follow a log-Euclidean method (22): Linear interpolation in log-space ensures smoothly varying symmetric positive-definite tensors with monotonically-varying determinants at any point in the growth process. At each intermediate pair of first fundamental forms, we compute the minimum-energy embedding corresponding to the interpolated bilayer metrics. To address the incompatibility of first and second fundamental forms at intermediate stages, we guide the growth process by prescribing four intermediate states, which serve as “way-points” for the growth trajectory (see *SI Appendix* for more details). In Fig. 2, *Left*, and *Movie S1*, we show a sequence of

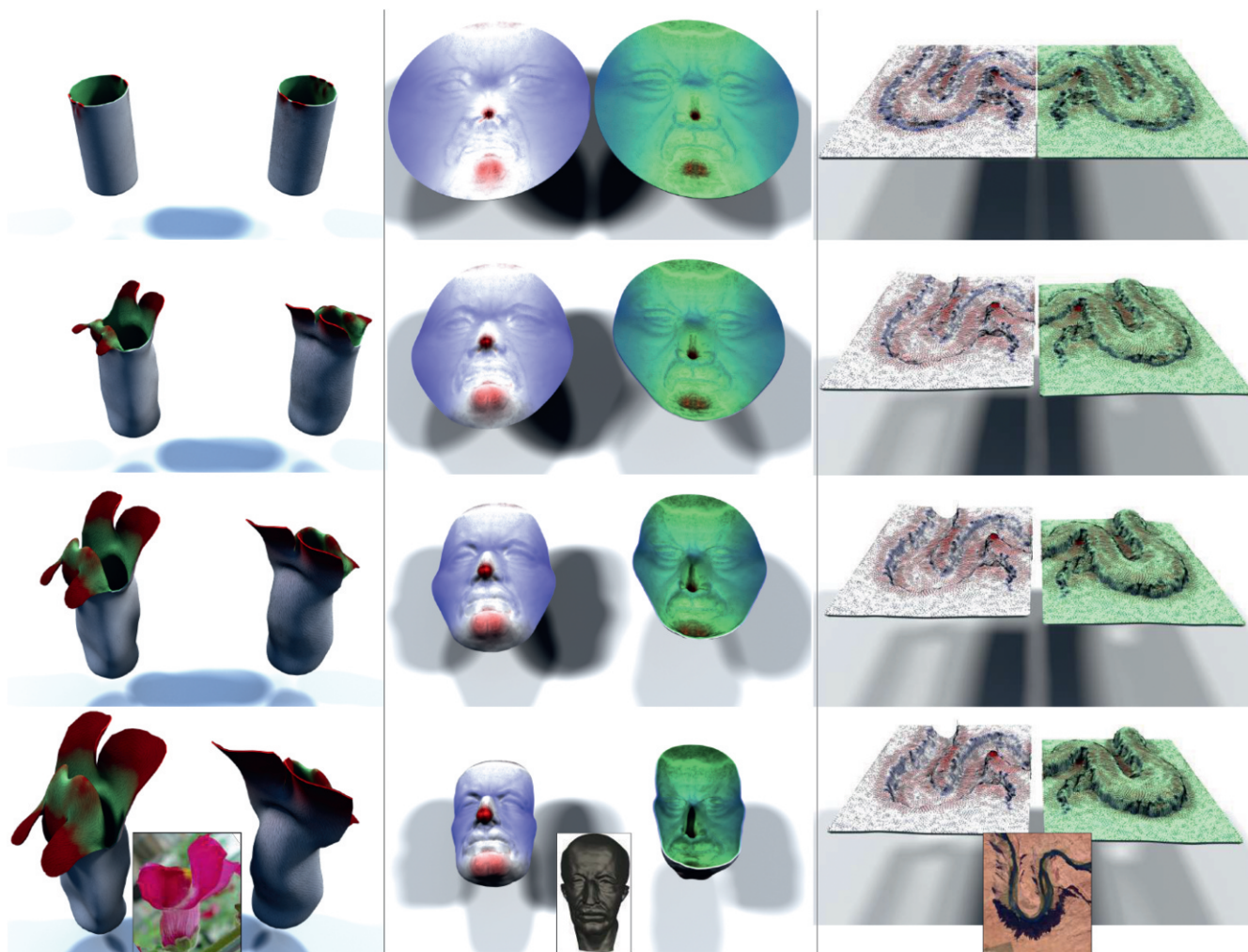


Fig. 2. Inverse design of vegetable, animal, and mineral surfaces. A snapdragon flower petal starting from a cylinder (*Left*), a face starting from a disk (*Center*), and the Colorado River horseshoe bend starting from a rectangle (*Right*). For each example, we show the initial state (top), the final state (bottom) and two intermediate grown states in between. In each state, the colors show the growth factors of the top (left) and bottom (right) layer, and the thin black lines indicate the direction of growth. The top layer is viewed from the front, and the bottom layer is viewed from the back, to highlight the complexity of the geometries. The target shape for each case is given in *Inset* at the bottom: a snapdragon flower (image courtesy of E. Coen); a computer-render of a bust of Max Planck (model is provided courtesy of Max Planck Institute for Informatics by the AIM@SHAPE Shape Repository); a satellite photo of the actual river bend (image courtesy of Google Earth). The height of the actual snapdragon flower is ~ 30 mm (19), whereas the depth of the canyon is 393 m according to USGS elevation data. (See *SI Appendix* for animations and details.)

intermediate shapes viewed from two different angles and, for comparison, the actual snapdragon flower.

To highlight the ability of our approach to capture complex surface geometries with features on multiple scales, we turn to the human face. In Fig. 2, *Center*, and *Movie S2*, we show that we can grow an initially flat bilayer disk into a 3D model of a human face, that of the physicist Max Planck. In this case, we linearly interpolate the growth factors from unity, on the initial disk, to their final values computed from Eq. 5, and show the result for energetic equilibria at two intermediate stages.

Finally, we use our inverse-design theory to grow a simulacrum of a complex inanimate surface, a horseshoe bend in the Colorado River in Arizona. Using United States Geological Survey (USGS) elevation data, we create our 3D target shape and grow it from a rectangular sheet. As in the snapdragon example, we use anchor points to guide the interpolation (see *SI Appendix* for more details). In Fig. 2, *Right*, and *Movie S3*, we show a sequence of intermediate shapes obtained during the growth process. These numerical results demonstrate the practical validity of our theoretical framework that allows us to capture the

shapes of complex absolute-scale-independent surfaces from the animal, vegetable, and mineral world.

Discussion

This study poses and solves the inverse-design problem of designing growth patterns for creating complex shapes from a uniformly thin isotropic elastic bilayer capable of sustaining orthotropic growth. It opens the way for formulating and solving other variants of the inverse-design problem for growth-metric tensors encountered in such cases as a single growing monolayer, isotropically growing bilayers (23), or the most general case of orthotropically growing bilayers with incompatible metrics, all of which will generally require numerical approaches for both the forward and inverse problems. The generalization to account for situations where the thicknesses of the two layers h_1 and h_2 are unequal (*SI Appendix*) provides yet another perspective, as this can be exploited for applications such as artificial lenses (24) or controlled actuation of the curvature in the presence of constraints. It is worth noting that in all of these situations, there are specific instances where the final residually strained state may

constitute an orbit of connected minima associated with a Goldstone mode, e.g., saddle-like solutions in heated or swollen plates (refs. 9 and 15, p. 158), but the general nature of these states and how to design them remains open.

Our approach is agnostic to the actual mechanism that induces this growth, whether it is heat, light, swelling, or biological growth, as long as it is mathematically equivalent to changing the metric of the constituent layers. While the experimental realization of bilayers is easy using additive manufacturing, achieving general orthotropic growth is currently more challenging. An existing technique for orthotropic growth relies on locally embedding fibrils in an isotropically growing base material, providing control over the angle between two fixed orthotropic swelling factors through the print direction (12). To also vary the other two degrees of freedom would require further control over

either the density of the fibrils in two orthogonal directions, or the density in one direction together with the isotropic growth factor of the base material, for each point in each layer. Alternatively, one could consider discrete lattice or origami-type surfaces that approximate the features of a continuous surface at a larger scale. This simplifies the problem by replacing the exact local control of growth by approximate control of an appropriate nonlocal average and is likely to be the first to be realizable experimentally.

ACKNOWLEDGMENTS. We thank E. Coen for the digital surface meshes and image of the snapdragon flower in Fig. 2. This work was supported in part by the Swiss National Science Foundation (to W.M.v.R.), National Science Foundation Grant DMS-1304211 (to E.V.), National Science Foundation Grant DMR 14-20570 (to L.M.), DMREF 15-33985 (to L.M.), and Army Research Office Grant W911NF-15-1-0166 (to L.M.).

- Liang H, Mahadevan L (2009) The shape of a long leaf. *Proc Natl Acad Sci USA* 106:22049–22054.
- Liang H, Mahadevan L (2011) Growth, geometry, and mechanics of a blooming lily. *Proc Natl Acad Sci USA* 108:5516–5521.
- Armon S, Efrati E, Kupferman R, Sharon E (2011) Geometry and mechanics in the opening of chiral seed pods. *Science* 333:1726–1730.
- Ben Amar M, Goriely A (2005) Growth and instability in elastic tissues. *J Mech Phys Solids* 53:2284–2319.
- Klein Y, Efrati E, Sharon E (2007) Shaping of elastic sheets by prescription of non-Euclidean metrics. *Science* 315:1116–1120.
- Dervaux J, Ben Amar M (2008) Morphogenesis of growing soft tissues. *Phys Rev Lett* 101:068101.
- Efrati E, Sharon E, Kupferman R (2009) Elastic theory of unconstrained non-Euclidean plates. *J Mech Phys Solids* 57:762–775.
- Lewicka M, Mahadevan L, Pakzad MR (2011) The Föppl-von Karman equations for plates with incompatible strains. *Proc R Soc A Math Phys Eng Sci* 467:402–426.
- Jones GW, Mahadevan L (2015) Optimal control of plates using incompatible strains. *Nonlinearity* 28:3153–3174.
- Kim J, Hanna JA, Byun M, Santangelo CD, Hayward RC (2012) Designing responsive buckled surfaces by halftone gel lithography. *Science* 335:1201–1205.
- Aharoni H, Sharon E, Kupferman R (2014) Geometry of thin nematic elastomer sheets. *Phys Rev Lett* 113:257801.
- Gladman AS, Matsumoto EA, Nuzzo RG, Mahadevan L, Lewis JA (2016) Biomimetic 4D printing. *Nat Mater* 15:413–418.
- Struik DJ (1988) *Lectures on Classical Differential Geometry* (Dover, New York), 2nd Ed.
- Weischedel C, Tuganov A, Hermansson T, Linn J, Wardetzky M (2012) Construction of discrete shell models by geometric finite differences (Fraunhofer ITWM, Kaiserslautern, Germany), Technical Report 220.
- Mansfield E (1989) *The Bending and Stretching of Plates* (Cambridge Univ Press, Cambridge, UK), 2nd Ed.
- do Carmo MP (1976) *Differential Geometry of Curves and Surfaces* (Prentice-Hall, Englewood Cliffs, NJ).
- Timoshenko S (1925) Analysis of bi-metal thermostats. *J Opt Soc Am* 11:233–255.
- Forterre Y, Skotheim JM, Dumais J, Mahadevan L (2005) How the Venus flytrap snaps. *Nature* 433:421–425.
- Green AA, Kennaway JR, Hanna AI, Bangham JA, Coen E (2010) Genetic control of organ shape and tissue polarity. *PLoS Biol* 8:e1000537.
- Kennaway R, Coen E, Green A, Bangham A (2011) Generation of diverse biological forms through combinatorial interactions between tissue polarity and growth. *PLoS Comput Biol* 7:e1002071.
- Coen E, Rebocho AB (2016) Resolving conflicts: Modeling genetic control of plant morphogenesis. *Dev Cell* 38:579–583.
- Arsigny V, Fillard P, Pennec X, Ayache N (2006) Log-Euclidean metrics for fast and simple calculus on diffusion tensors. *Magn Reson Med* 56:411–421.
- Pezzulla M, Smith GP, Nardinocchi P, Holmes DP (2016) Geometry and mechanics of thin growing bilayers. *Soft Matter* 12:4435–4442.
- Lee LP (2005) Inspirations from biological optics for advanced photonic systems. *Science* 310:1148–1150.